



# Excitation of graphene surface plasmons polaritons by guided-mode resonances with high efficiency

YUXIANG REN,<sup>1</sup> XUGUANG GUO,<sup>1,\*</sup>  GUIXUE ZHANG,<sup>1</sup> ALEXEY V. BALAKIN,<sup>1,3,4</sup>  ALEXANDER P. SHKURINOV,<sup>1,3,4</sup> ANQI YU,<sup>1,2</sup> AND YIMING ZHU<sup>1,2,5</sup>

<sup>1</sup>Terahertz Technology Innovation Research Institute, Terahertz Spectrum and Imaging Technology Cooperative Innovation Center, Shanghai Key Lab of Modern Optical System, University of Shanghai for Science and Technology, 516 Jungong Road, Shanghai 200093, China

<sup>2</sup>Shanghai Institute of Intelligent Science and Technology, Tongji University, Shanghai 200093, China

<sup>3</sup>Faculty of Physics and International Laser Center, Lomonosov Moscow State University, Leninskie Gory 1-2, Moscow 19991, Russia

<sup>4</sup>ILIT RAS – Branch of the FSRC “Crystallography and Photonics” RAS, Svyatoozerskaya 1, 140700 Shatura, Moscow Region, Russia

<sup>5</sup>ymzhu@usst.edu.cn

\*xgguo\_sh@qq.com

**Abstract:** An Otto-like configuration for the excitation of graphene surface plasmon polaritons (GSPPs) is proposed. The configuration is composed of a metallic grating-dielectric-waveguide structure and a monolayer graphene with a subwavelength vacuum gap between them. The evanescent field located at the bottom surface of the dielectric waveguide corresponding to grating-coupled guided-mode resonances (GMRs) is utilized to efficiently excite the highly confined GSPPs. The finite difference time domain method is used to investigate the behaviors of the GMR-GSPP hybrid modes. The dispersion relations of GMRs and GSPPs are calculated and the numerical results further identify the excitation of GMR-GSPP hybrid modes. By changing the gap between the graphene layer and the bottom of the dielectric waveguide and the Fermi energy of graphene, the resonant frequencies of GMR-GSPP hybrid modes can be continuously tuned. When the optimized excitation condition is satisfied, the maximum energy enhancement factor in the gap can reach about 500 at the resonant frequencies. The proposed structure can be used to realize highly sensitive, compatible with planar fabrication technology, and electrically (mechanically) tunable sensors.

© 2020 Optical Society of America under the terms of the [OSA Open Access Publishing Agreement](#)

## 1. Introduction

Graphene surface plasmon polaritons (GSPPs) have attracted much attention because of their low dissipation, strong localization, and tunable resonant frequencies [1–3]. Due to the mismatch of the dispersion relations, the GSPPs cannot be directly launched by the incident electromagnetic waves propagating in free space. Because the dispersion curve of GSPP is always lying to the right of the light line, additional wavevector compensation needs to be introduced to excite the GSPPs. Previous studies have shown that the excitation of the GSPPs by grating coupling [4–6] is one of the most common methods to solve the momentum mismatch. The basic idea is that the evanescent diffraction modes supported by gratings can provide large in-plane momentums for p-polarized incident electromagnetic waves. Another widely-used way to overcome the mismatch of wavevector is through the prism coupling scheme (Otto and Kretschmann-Raether configurations) [7], in which the incident light (p-polarized) passing through the prism with a higher index of refraction suffers total internal reflection on the surface as well as the generation

of evanescent waves to meet the wavevector match condition of GSPPs. With the development of near-field optics, the compensation of wavevector can also be provided by the near-field evanescent fields by using metal tips of scanning near-field optical microscopes [8,9]. There are also other ways to excite GSPPs, such as by using electron beams [10], dipolar sources [11], and the patterned graphene [12]. The graphene-based devices have potential applications in bio-sensing and active functional devices [13–18].

Recently, various phenomena related to the coupling between two electromagnetic modes, for example, electromagnetically induced transparency [19–21], Fano resonance [22,23], and hybrid plasmonic-photonic resonators [24,25], have attracted many interests and attentions. Hayashi *et al.*, have demonstrated a structure composed of a prism, a thin metal layer, and a multilayer dielectric waveguide, in which the guided-mode resonances (GMRs) can be effectively launched by the prism-induced SPPs [26,27]; and because of the coupling between the SPPs and the GMRs, the electromagnetic energy is effectively transferred from the SPP modes to the GMR modes, which results in a strong enhancement of field in the waveguide. Subsequently, Hua *et al.*, have proposed a planar structure composed of a metallic grating and a multilayer dielectric waveguide to investigate the coupling of SPPs and GMRs and the energy localization in the waveguide [28]. In the above investigations, the SPPs are directly excited, and due to the evanescent field-mediated coupling between SPPs and GMRs, the GMRs are indirectly launched. However, the inverse case has not been studied.

In this paper, strongly coupled GMR-GSPP hybrid modes supported by a planar structure are theoretically investigated. The structure consists of a silver grating, a slab dielectric (Si) waveguide, a subwavelength vacuum gap, and a monolayer graphene (from top to bottom). Through the metallic grating, the normally-incident transverse-magnetic (TM) waves with the electric field direction perpendicular to the metallic strips are effectively coupled into the GMR modes of the slab dielectric waveguide at resonant frequencies. The GMR modes suffer total internal reflection at the waveguide/vacuum interface, which leads to the generation of evanescent fields in the vacuum gap. When the energy and momentum conservation conditions are both satisfied, the evanescent-field-mediated GMR-GSPP modes can be launched and the electromagnetic energy is effectively squeezed into the subwavelength vacuum gap. Different from the conventional low-quality-factor GSPPs, the strongly-coupled GMR-GSPP hybrid modes introduce very sharp features in the reflection spectra. Meanwhile, the electromagnetic energies associated with the GMR-GSPP modes are mainly localized in the gap, which results in a higher energy enhancement factor. Compared with the prism coupling scheme, the proposed structure is compatible with the planar-integration techniques and no precise angle control is needed to launch the GMR-GSPP modes. In addition, by changing the dimension of the gap and Fermi energy of graphene, the resonant frequencies of GMR-GSPP mode can be tuned. All the above features are beneficial for realizing high-performance sensors.

## 2. Results and discussion

As shown in Fig. 1(a), the proposed device consists of a straight silver grating, a slab dielectric waveguide, a subwavelength vacuum gap, and a free-standing monolayer graphene. For simple clarity, the substrate to support the monolayer is not included. The periodicity, duty cycle, and strip height of the grating, are  $p=69\ \mu\text{m}$ , 50%, and  $1\ \mu\text{m}$ , respectively. The thickness of the slab waveguide is  $46\ \mu\text{m}$ , and the relative dielectric constant is 12.25 (lossless silicon). A commercial electromagnetic simulation package based on finite difference time domain method (FDTD) [29] is used to compute the reflectance and field distribution. The relative dielectric constant of silver is described by the Drude model,

$$\varepsilon(\omega) = 1 - \frac{\omega_p^2}{\omega^2 + i\gamma\omega} \quad (1)$$

where the parameters used in the Drude model for silver are plasma frequency  $\omega_p=1.37\times 10^{16}$  rad·s<sup>-1</sup> and the scattering rate  $\gamma=7.29\times 10^{13}$  rad·s<sup>-1</sup> [30],  $\omega$  is the angular frequency of the incident light, and  $i$  is the imaginary unit. In the terahertz frequency range, the imaginary part can be omitted, because silver can be treated as a perfect electric conductor. Then, Eq. (1) can be simplified as  $\varepsilon(\omega)=1-\omega_p^2/\omega^2$ . The driving source is TM electromagnetic waves with the polarization direction perpendicular to the grating strip.

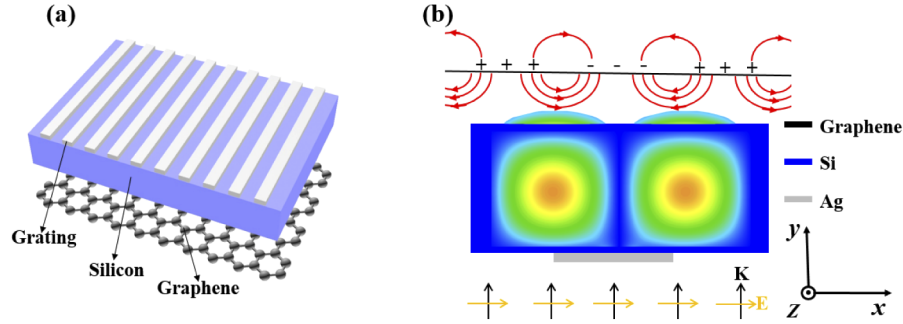


**Fig. 1.** (a) The schematic of the proposed structure, and (b) the principle of the excitation of GMR-GSPP modes.

Graphene is considered as a surface conductive sheet with zero thickness in numerical calculations, and its conductivity can be expressed as the sum of the intraband term  $\sigma_{intra}$  and the interband term  $\sigma_{inter}$ . Nevertheless, due to the Pauli blocking, the interband term can be neglected at terahertz frequencies on account of the photon energy  $\hbar\omega \ll 2E_F$ , where  $E_F$  is the Fermi energy. The conductivity of graphene is well expressed by the Drude-like model [31,32]

$$\sigma = \frac{ie^2k_B T}{\pi\hbar^2(\omega + \frac{2i}{\tau})} \ln \left[ \exp\left(-\frac{E_F}{2k_B T}\right) + \exp\left(\frac{E_F}{2k_B T}\right) \right] \quad (2)$$

where  $\tau$  is the relaxation time,  $e$  is the electron charge,  $T$  is the temperature in Kelvin,  $\hbar$  is the reduced Planck constant, and  $k_B$  is the Boltzmann constant.

The excitation of GMRs in the grating-waveguide structure is firstly explored. Since the metallic grating will introduce an additional phase, a very low grating duty cycle of 10% is selected to diminish the effects of grating on the GMRs. A TM electromagnetic wave with the polarization perpendicular to the metallic strip is used as the driving source. When the incident light impinges on the grating, at some frequencies, if the in-plane-wavevector-frequency relations of diffraction modes satisfy the dispersion relations of GMRs, the GMRs will be launched. As shown in Fig. 2(a), the reflection spectrum of the grating-waveguide structure is computed with the Lumerical FDTD package. Floquet periodic boundary conditions are used on the left and right sides of the computational domain, and two perfect match layers are added to absorb the transmission and reflection waves. The broad periodic reflection peak-dip structure is due to the Fabry-Perot interference. A series of sharp Fano-shaped features are superimposed on the peak-dip structure, which correspond to the launch of GMRs. In order to further identify these sharp Fano-shaped reflection features, the dispersion relation of GMR is numerically calculated. Without considering the effects of grating, the transcendental equation for the dispersion relations of GMR are,

$$\tan(\kappa d) = \frac{n_1^2 \kappa^2 (n_3^2 \gamma + n_2^2 \delta)}{n_2^2 n_3^2 \kappa^2 - n_1^4 \gamma \delta} \quad (3)$$

$$\kappa = (n_1^2 k^2 - \beta^2)^{\frac{1}{2}} \quad (4)$$

$$\gamma = (\beta^2 - n_2^2 k^2)^{\frac{1}{2}} \quad (5)$$

$$\delta = (\beta^2 - n_3^2 k^2)^{\frac{1}{2}} \quad (6)$$

where  $d$  and  $n_1$  are the thickness and the refractive constant of the slab dielectric waveguide, respectively.  $n_2$  ( $n_3$ ) is the refractive constant of above (below) environment of the waveguide.  $\beta=2\pi m/p$  is the wavevector provided by the metallic gratings with  $m$  an integer. Figure 2(b) shows the dispersion relations for the first four order GMR modes. Comparing Figs. 2(a) and 2(b), it is obvious that the frequencies of the Fano-shaped features in Fig. 2(a) correspond to those of the intersection points of the black solid lines (dispersion-relation curves) and the dotted orange lines (the in-plane wavevectors provided by the grating) in Fig. 2(b). Then it can be concluded that a GMR mode will be launched if its momentum matches with that offered by the metallic gratings.

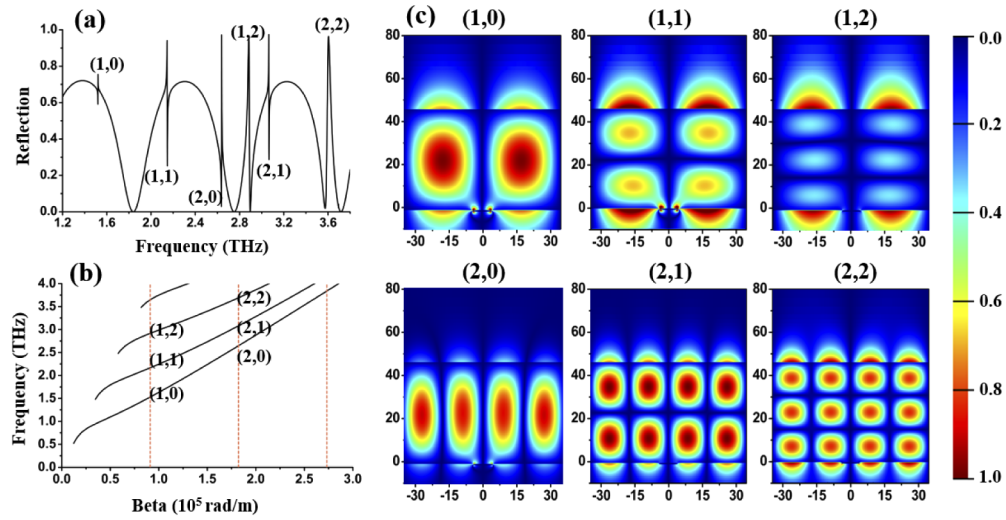


**Fig. 2.** (a) Reflection spectrum of the grating-waveguide structure, (b) the first four order dispersion relations (solid black lines) of GMRs supported by the dielectric waveguide and finite wavevectors (dotted orange lines) provided by the coupling grating, (c) the distributions of electric field  $|E_y|$  for different Fano-shaped reflection features labeled as  $(m,n)$  shown in (a) with  $m=1,2$  and  $n=0,1,2$ , respectively.

Aided by the results shown in Fig. 2(b), the origins of the Fano-shaped features shown in Fig. 2(a) are all well addressed. In order to further explore the characteristics of the GMRs, the intersection points in Fig. 2(b) are labeled as  $(m,n)$  with  $m$  the diffraction mode order of grating and  $n$  the GMR order, and the corresponding electric field distributions  $|E_y|$  are shown in Fig. 2(c). Obviously, for the  $(m,n)$  GMR mode, the node number of  $|E_y|$  is  $m$  in  $x$  direction and  $n$  in  $y$  direction. In addition, accompanied with the excitation of GMRs, there are strong evanescent fields on two surfaces of the grating-waveguide structure, which is similar to the case of prism-coupled GSPPs.

To find the phase match condition of GMR-launched GSPP, the dispersion relation of GSPP is numerically calculated by solving the transcendental equation [6,33],

$$\frac{\varepsilon_{r1}}{\sqrt{\beta^2(\omega) - \varepsilon_{r1}k_0^2}} + \frac{\varepsilon_{r2}}{\sqrt{\beta^2(\omega) - \varepsilon_{r2}k_0^2}} = -\frac{i\sigma(\omega)}{\varepsilon_0\omega} \quad (7)$$

where  $\varepsilon_{r1}$  ( $\varepsilon_{r2}$ ) is the dielectric constant of the material above (below) the graphene layer,  $\beta(\omega)$  is the in-plane wavevector of GSPP,  $k_0=2\pi/\lambda$  is the vacuum wavevector with  $\lambda$  the vacuum

wavelength, and  $\varepsilon_0$  is the vacuum permittivity. The monolayer graphene has a metal-like response to in-plane electric field and a dielectric-like response to the surface-normal electric field. The dispersion relation of GSPP is different from that of other type of two-dimensional (2D) electron gases [34], due to the massless electrons in graphene.

With a carrier relaxation time of  $\tau=5$  ps,  $E_F=0.35$  eV, and  $\varepsilon_{r1}=\varepsilon_{r2}=1.0$ , the dispersion relations of GSPP and GMRs are first numerically calculated and plotted in Fig. 3(a). There are two intersection points at about 2.17 THz and 3.10 THz between the dispersion curves of GSPP and the first-order GMR. The wavevector of the first intersection point is very close to that of the grating first-order diffraction mode, which indicates that the hybrid GMR-GSPP mode can be effectively launched by the metallic grating.

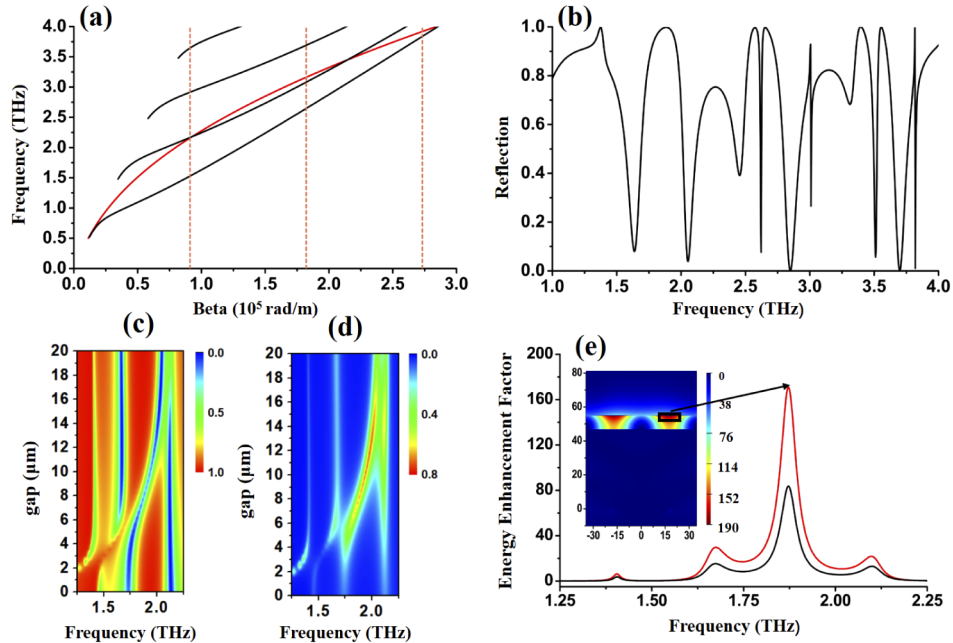


**Fig. 3.** (a) Dispersion relations of GSPP and GMRs with  $\tau=5$  ps,  $E_F=0.35$  eV, (b) reflection spectrum of the grating-waveguide structure with grating duty cycle of 50%, (c), (d) false-color contours of reflection and absorption spectra with the gap height  $h$  in the range of 0–20  $\mu\text{m}$ , (e) the energy enhancement factor spectrum in the gap with  $h=8$   $\mu\text{m}$ , black line: averaged in the whole gap region, red line: averaged in the labeled high-field region, the illustration is the electric field distribution  $|E_y|^2$  at 1.85 THz, where the corresponding energy enhancement factor in the gap reaches its maximum value.

In order to study the energy enhancement in the gap between the slab dielectric waveguide and the monolayer graphene, an energy enhancement factor  $\gamma_E$  is defined as,

$$\gamma_E = \frac{|E_{rec}|^2}{|E_{inc}|^2} \quad (8)$$

where  $E_{rec}$  is the volume-averaged field in the rectangle region, and  $E_{inc}$  is the area-averaged incident field. To further explore the behaviors of the hybrid GMR-GSPP mode, the dependences of reflection spectrum, electric field distribution, and the energy enhancement factor on the gap height  $h$  (the distance between the bottom surface of the waveguide and the monolayer graphene) are systemically investigated. The duty cycle of the metallic grating is set to 50% for improving the coupling efficiency, and the other parameters are same with the case shown in Fig. 2(a). Due

to the influence of metallic grating with finite duty cycle, as shown in Fig. 3(b), there are obvious differences between 10% and 50% duty cycles in terms of resonant frequencies and dip widths of the reflection features. In the frequency range of 1.3-2.2 THz, there are three reflection dips at 1.48 THz, 1.75 THz, and 2.17 THz, respectively. When the monolayer graphene is introduced, a new reflection dip corresponding to the excitation of GSPP appears for the gap width  $h > 2.0 \mu\text{m}$  (Fig. 3(c)). Because the gap width is in deep subwavelength scale, the grating-waveguide structure can be seen by the GSPP. Therefore, the dielectric constant  $\epsilon_{r2}$  below the graphene layer in Eq. (4) must be replaced by an effective dielectric constant  $\epsilon_{eff}$ . It has been shown in Refs. [7,35–36] that the value of  $\epsilon_{eff}$  decreases with increasing the gap width, which leads to the blue shift of GSPP at the same wavevector (Fig. 3(c)). Therefore, the intersection points between the dispersion curves of GMR and GSPP modes can be tuned by changing the gap width. Meanwhile, due to the strong interaction between GSPP and GMR modes via near-field coupling, there are three anti-crossing regions, which indicates that the hybrid GMR-GSPP modes are launched in the anti-crossing regions.

The false-color contour of absorption spectrum with the gap width of 0-20  $\mu\text{m}$  is shown in Fig. 3(d), which is directly related to the electric field intensity near the graphene layer because the monolayer graphene is the only lossy material in the structure. When the gap width is larger than 7  $\mu\text{m}$ , a strong absorption is followed by the excitation of GSPP. The energy enhancement factor spectra with  $h=8 \mu\text{m}$  are calculated and plotted in Fig. 3(e). The black dot-dash line represents the energy enhancement factor averaged in the whole gap region, and the red solid line represents the one averaged in the high-field region labeled by a black square in Fig. 3(e). The shapes of the two curves are similar with each other. At 1.85 THz, the two energy enhancement factors reach their maximum values of about 84 and 171, respectively. The electric field distribution of  $|E_y|^2$  at 1.85 THz is shown in the insertion of Fig. 3(e). The field distribution shows that the GMR-GSPP mode is launched by the (1,1) GMR mode, which is in accordance with the numerical dispersion relations shown in Fig. 3(a). The field energy is mostly located in the gap, which is very different from the traditional GSPP that the field energy is symmetrically located at both sides of the monolayer graphene. Two reasons should be responsible for such a field distribution. The first reason is that the value of the effective refractive constant  $\epsilon_{eff}$  is larger than that of  $\epsilon_{r1}$ , and the field energy tends to locate at the side having higher refractive constant. The second one is that the field distribution is determined by the hybrid GMR-GSPP mode, which has the mixed characteristics of GMR- and GSPP-related field distributions. Moreover, as shown in Figs. 3(c) and 3(d), the GMR-GSPP mode is on the GSPP-like branch, which results in the GSPP-dominant electric field distribution. The strong field enhancement in a deep subwavelength cavity is very important to study the strong light-matter interactions and construct sensors with high sensitivity.

Based on the same principle presented in Fig. 3(a), the frequencies of GMR-GSPP modes can be tuned by changing the Fermi energy of graphene. As the Fermi energy increases, the dispersion relation curve of GSPP shifts to higher frequency at a fixed wavevector. By introducing a capacitor-like structure and the monolayer graphene as an electrode, the Fermi energy can be altered via a direct bias voltage. Figure 4 presents the false-color contours of reflection and absorption spectra in the frequency range of 1.25-2.50 THz with the Fermi energy of 0-1 eV and a fixed medium gap width of 5.5  $\mu\text{m}$ . Similar anti-crossing behaviors between the GMR modes and the GSPP mode appear. At  $E_F=0.5 \text{ eV}$  and about 2.0 THz, the largest anti-crossing gap of about 0.2 THz appears. In this anti-crossing region, the intensive absorption (Fig. 4(b)) represents the highly efficient excitation of hybrid GMR-GSPP mode. The simulation results shown in Fig. 4 indicate that except for the gap width, Fermi energy is another important parameter to tune the resonant frequencies and to maximize the energy enhancement factor in the gap region.

An improved optimization procedure is adopted to search the best excitation condition of GMR-GSPP modes by solving the dispersion relation transcendental equations of GMRs and GSPP. The 2D parameter space ( $E_F, \epsilon_{eff}$ ) is roughly swept. In consideration of calculation

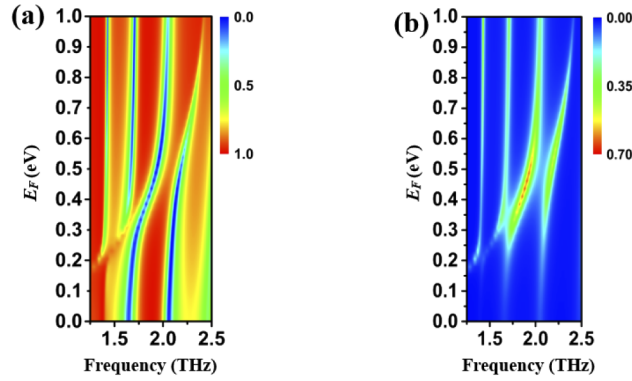


**Fig. 4.** The false-color contours of reflection (a) and absorption (b) spectra with Fermi energy in the range of 0-1 eV and a fixed gap value of 5.5  $\mu\text{m}$ .

precision, we do not calculate the value of  $\varepsilon_{eff}$  as a function of gap width  $h$ . Instead, when the parameter ( $E_F, \varepsilon_{eff}$ ) is determined, the gap width  $h$  is scanned. Figure 5(a) shows the optimized dispersion relations of GMRs and GSPP at the 2D parameter point (0.5 eV, 1.375). There is a long coincidence region between the dispersion relation curves of GSPP and the first-order GMR, which makes the excitation condition of GMR-GSPP modes be satisfied more easily.

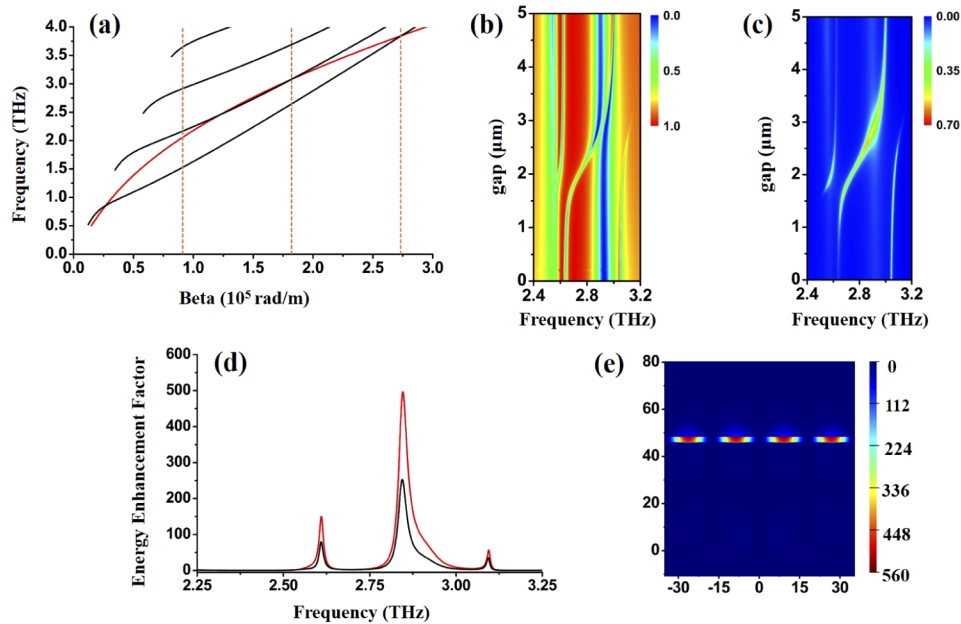


**Fig. 5.** (a) Dispersion relations of GSPP and GMRs with  $\tau=5$  ps,  $E_F=0.5$  eV, the reflection (b) and absorption (c) spectra with the gap width in the range of 0-5  $\mu\text{m}$ , (d) the energy enhancement factor spectra in the gap with  $h=2.5$   $\mu\text{m}$ , black line: averaged in the whole gap region, red line: averaged in the labeled high-field region, and (e) the electric field distribution  $|E_y|^2$  at 2.85 THz, where the corresponding energy enhancement factor in the gap reaches its maximum value.

In Figs. 5(b) and 5(c), the false-color contours of reflection and absorption spectra are depicted with the gap width  $h=0-5$   $\mu\text{m}$  and a fixed Fermi energy  $E_F=0.5$  eV. In comparison with Fig. 3(c),

due to a higher value of Fermi energy, the anti-crossing regions occur with smaller gap widths. It is expected that a small gap width is beneficial for increasing the excitation efficiency of GMR-GSPP modes and the energy enhancement factor in the gap. From Fig. 5(c), the hybrid GMR-GSPP modes are launched at about  $h=2.0\ \mu\text{m}$  and  $h=2.5\ \mu\text{m}$ , and at the later gap width, a higher energy enhancement factor should be obtained. The energy enhancement factor spectrum with  $E_F=0.5\ \text{eV}$  and  $h=2.5\ \mu\text{m}$  is calculated and shown in Fig. 5(d). At 2.85 THz, the two energy enhancement factors reach their maximum values of 251 and 496, respectively. The related mode field distribution  $|E_y|^2$  is shown in Fig. 5(e). The electric field energy is effectively squeezed into the gap. The field distribution indicates the hybrid mode is launched by the (2,1) GMR mode. The hybrid mode corresponding to the first anti-crossing region is excited by the (1,1) GMR mode. It is noticeable that because of the influence of the metallic grating, there is a remarkable discrepancy between the dispersion relation calculations and the full-wave FDTD simulations to obtain the resonant frequencies of GMR-GSPP modes. However, the dispersion relation calculations are valuable for understanding the excitation principle and determining the approximate resonant frequencies of hybrid GMR-GSPP modes.

Due to the large difference in loss (quality factor) between the near lossless GMR and the lossy GSPP, there is a remarkable difference between GMR-GSPP and GSPP-GMR modes. Such a difference can be explained by using the coupled oscillator model [37]. For GSPP-GMR hybrid modes, the driven source is directly applied to the lossy GSPP, and the near-field coupling between the GSPP and GMR results in a sharp reflection peak located in a broad reflection dip. The GSPP-GMR hybrid modes have been widely investigated. On the contrary, for GMR-GSPP, the excitation process is inverse, which results in a sharp reflection dip in the high reflection background. As far as sensing is concerned, the GMR-GSPP structure may be more robust to measurement noise, and less electromagnetic energy is absorbed by the device.

The intrinsic relaxation time in graphene is much longer than the set value of  $\tau=5\ \text{ps}$ . However, due to the existence of extrinsic scattering centers, for example, dopants in graphene, ionized impurity and phonon in substrate, it is not an easy task to obtain a monolayer graphene with  $\tau=5\ \text{ps}$  experimentally. Therefore, the effects of carrier relaxation time are explored, and the numerical results are shown in Fig. 6. In order to demonstrate the anti-crossing behavior more clearly, a higher value of  $E_F=0.7\ \text{eV}$  is selected. For  $\tau>1\ \text{ps}$ , Figs. 6(a) and 6(b) show that the reflection spectra are quite similar. However, with further decreasing of  $\tau$  to 0.2 ps, due to the broadening of reflection dips, the anti-crossing region is smeared (Fig. 6(c)). As shown in Fig. 6(d), the energy enhancement factor is much sensitive to the carrier relaxation time. The

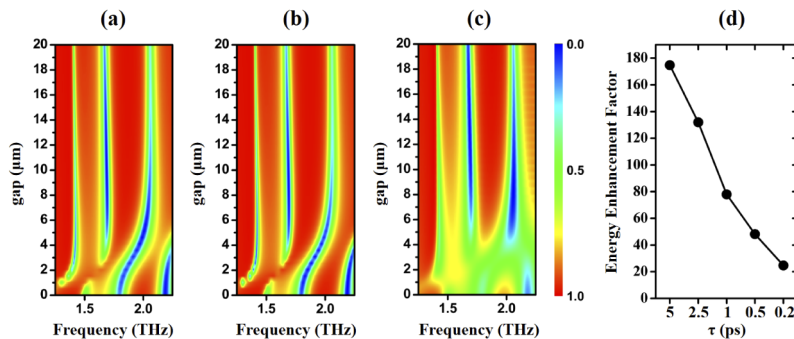


**Fig. 6.** The false-color contours of reflection spectra with  $E_F=0.7\ \text{eV}$  and  $\tau=5\ \text{ps}$  (a), 1 ps (b), and 0.2 ps (c). (d) The maximum energy enhancement factor as a function of carrier relaxation time at 1.85 THz with Fermi energy  $E_F$  and gap height  $h$  as optimization parameters.

energy enhancement factor linearly decreases from 171 to 21 with  $\tau$  decreasing from 5 to 0.2 ps, which may be due to the decrease of coupling strength between the GMR and GSPP modes and the enhancement of absorption in graphene.

Because it is very difficult to fabricate the free-standing monolayer graphene. The effects of a semi-infinite substrate (benzocyclobutene, BCB, dielectric constant: 2.65) is checked. The numerical results show that the electromagnetic energy is still located in the vacuum gap, and the main conclusions are not influenced.

### 3. Conclusion

A combined structure, composed of a metallic grating on a slab dielectric waveguide structure and a monolayer graphene with a subwavelength vacuum gap between them, is studied. Hybrid GMR-GSPP modes can be effectively launched via an Otto-like configuration. The excitation conditions for GMR-GSPP modes are qualitatively revealed by solving the dispersion relation transcendental equations of GMR and GSPP. Full-wave simulations with Lumerical FDTD package further identify the above excitation conditions. Strong interaction between the GMR and GSPP modes leads to the anti-crossing behavior in the reflection spectra by changing the gap width and Fermi energy of graphene. With the excitation of hybrid GMR-GSPP modes, the incident electromagnetic energy can be effectively funneled into the gap and a large volume-averaged energy enhancement factor of about 500 is obtained in the gap. The proposed structure can be used to realize highly sensitive, compatible with planar fabrication technology, and electrically (mechanically) tunable sensors.

### Funding

National Natural Science Foundation of China (61731020,61722111); National Key Research and Development Program of China (2017YFA0701005); Higher Education Discipline Innovation Project (D18014); Science and Technology Commission of Shanghai Municipality (17590750300); Science and Technology Commission of Shanghai Municipality (YDZX20193100004960); Russian Academy of Sciences (075-15-2019-1950).

### Disclosures

The authors declare no conflicts of interest.

### References

1. J. Christensen, A. Manjavacas, S. Thongrattanasiri, F. H. L. Koppens, and F. J. G. Abajo, "Graphene plasmon waveguiding and hybridization in individual and paired nanoribbons," *ACS Nano* **6**(1), 431–440 (2012).
2. E. H. Hwang and S. D. Sarma, "Dielectric function, screening, and plasmons in two-dimensional graphene," *Phys. Rev. B* **75**(20), 205418 (2007).
3. L. Brey and H. A. Fertig, "Elementary electronic excitations in graphene nanoribbons," *Phys. Rev. B* **75**(12), 125434 (2007).
4. L. Ju, B. S. Geng, J. Horng, C. Girit, M. Martin, Z. Hao, H. A. Bechtel, X. G. Liang, A. Zettl, Y. R. Shen, and F. Wang, "Graphene plasmonics for tunable terahertz metamaterials," *Nat. Nanotechnol.* **6**(10), 630–634 (2011).
5. N. M. R. Peres, Y. V. B. Ludov, A. Ferreira, and M. I. Vasilevskiy, "Exact solution for square-wave grating covered with graphene: surface plasmon-polaritons in the terahertz range," *J. Phys.: Condens. Matter* **25**(12), 125303 (2013).
6. W. L. Gao, J. Shu, C. Y. Qiu, and Q. F. Xu, "Excitation of Plasmonic Waves in Graphene by Guided-Mode Resonances," *ACS Nano* **6**(9), 7806–7813 (2012).
7. Y. V. Bludov, A. Ferreira, N. M. R. Peres, and M. I. Vasilevskiy, "A primer on surface plasmon-polaritons in graphene," *Int. J. Mod. Phys. B* **27**(10), 1341001 (2013).
8. J. N. Chen, M. Badioli, P. A. González, S. Thongrattanasiri, F. Huth, J. Osmond, M. Spasenovic, A. Centeno, A. Pesquera, P. Godignon, A. Z. Elorza, N. Camara, F. J. G. Abajo, R. Hiltenbrand, and F. H. L. Koppens, "Optical nano-imaging of gate-tunable graphene plasmons," *Nature* **487**(7405), 77–81 (2012).
9. Z. Fei, A. S. Rodin, G. O. Andreev, W. Bao, A. S. Mcleod, M. Wagner, L. M. Zhang, Z. Zhao, M. Thiemens, G. Dominguez, M. M. Fogler, A. H. C. Neto, C. N. Lau, F. Keilmann, and D. N. Basov, "Gate-tuning of graphene plasmons revealed by infrared nano-imaging," *Nature* **487**(7405), 82–85 (2012).

10. T. Zhao, M. Hu, R. B. Zhong, S. Gong, C. Zhang, and S. G. Liu, "Cherenkov terahertz radiation from graphene surface plasmon polaritons excited by an electron beam," *Appl. Phys. Lett.* **110**(23), 231102 (2017).
11. F. H. L. Koppens, D. E. Chang, and F. J. G. Abajo, "Graphene plasmonics: a platform for strong light-matter interactions," *Nano Lett.* **11**(8), 3370–3377 (2011).
12. H. Huang, S. L. Ke, B. Wang, H. Long, K. Wang, and P. X. Lu, "Numerical study on plasmonic absorption enhancement by a rippled graphene sheet," *J. Lightwave Technol.* **35**(2), 320–324 (2017).
13. G. G. Zheng, J. W. Cong, Y. Y. Chen, L. H. Xu, and S. R. Xiao, "Angularly dense comb-like enhanced absorption of graphene monolayer with attenuated-total-reflection configuration," *Opt. Lett.* **42**(15), 2984–2987 (2017).
14. J. C. Wang, L. Yang, Z. D. Hu, W. J. He, and G. G. Zheng, "Analysis of graphene-based multilayer comb-like absorption system based on multiple waveguide theory," *IEEE Photonics Technol. Lett.* **31**(7), 561–564 (2019).
15. L. F. Ye, F. Zeng, Y. Zhang, and Q. H. Liu, "Composite graphene-metal microstructures for enhanced multiband absorption covering the entire terahertz range," *Carbon* **148**, 317–325 (2019).
16. L. F. Ye, K. H. Sui, Y. H. Liu, M. Zhang, and Q. H. Liu, "Graphene-based hybrid plasmonic waveguide for highly efficient broadband mid-infrared propagation and modulation," *Opt. Express* **26**(12), 15935–15947 (2018).
17. L. F. Ye, K. H. Sui, and H. Feng, "High-efficiency couplers for graphene surface plasmon polaritons in the mid-infrared region," *Opt. Lett.* **45**(2), 264–267 (2020).
18. L. F. Ye, K. H. Sui, Y. Zhang, and Q. H. Liu, "Broadband optical waveguide modulators based on strongly coupled hybrid graphene and metal nanoribbons for near-infrared applications," *Nanoscale* **11**(7), 3229–3239 (2019).
19. S. E. Harris, "Electromagnetically induced transparency," *Phys. Today* **50**(7), 36–42 (1997).
20. M. Fleischhauer, A. Imamoglu, and J. P. Marangos, "Electromagnetically induced transparency: Optics in coherent media," *Rev. Mod. Phys.* **77**(2), 633–673 (2005).
21. S. Y. Xiao, T. Wang, T. T. Liu, X. C. Yan, Z. Li, and C. Xu, "Active modulation of electromagnetically induced transparency analogue in terahertz hybrid metal-graphene metamaterials," *Carbon* **126**, 271–278 (2018).
22. B. Luk'yanchuk, N. I. Zheludev, S. A. Maier, N. J. Halas, P. Nordlander, H. Giessen, and C. T. Chong, "The Fano resonance in plasmonic nanostructures and metamaterials," *Nat. Mater.* **9**(9), 707–715 (2010).
23. A. E. Miroshnichenko, S. Flach, and Y. S. Kivshar, "Fano resonances in nanoscale structures," *Rev. Mod. Phys.* **82**(3), 2257–2298 (2010).
24. X. D. Yu, L. Shi, D. Z. Han, J. Zi, and P. V. Braun, "High quality factor metallodielectric hybrid plasmonic-photonic crystals," *Adv. Funct. Mater.* **20**(12), 1910–1916 (2010).
25. M. Chamanzar and A. Adibi, "Hybrid nanoplasmonic-photonic resonators for efficient coupling of light to single plasmonic nanoresonators," *Opt. Express* **19**(22), 22292–22304 (2011).
26. S. Hayashi, D. V. Nesterenko, and Z. Sekkat, "Waveguide-coupled surface plasmon resonance sensor structures: Fano lineshape engineering for ultrahigh-resolution sensing," *J. Phys. D: Appl. Phys.* **48**(32), 325303 (2015).
27. S. Hayashi, D. V. Nesterenko, A. Rahmouni, and Z. Sekkat, "Observation of Fano line shapes arising from coupling between surface plasmon polariton and waveguide modes," *Appl. Phys. Lett.* **108**(5), 051101 (2016).
28. H. Lu, X. T. Gan, D. Mao, B. H. Jia, and J. L. Zhao, "Flexibly tunable high-quality-factor induced transparency in plasmonic systems," *Sci. Rep.* **8**(1), 1–9 (2018).
29. The FDTD Solutions Trademark Software: [www.lumerical.com](http://www.lumerical.com).
30. H. Shin, P. B. Catrysse, and S. H. Fan, "Effect of the plasmonic dispersion relation on the transmission properties of subwavelength cylindrical holes," *Phys. Rev. B* **72**(8), 085436 (2005).
31. P. Y. Chen and A. Alu, "Atomically thin surface cloak using graphene monolayers," *ACS Nano* **5**(7), 5855–5863 (2011).
32. G. W. Hanson, "Dyadic Green's functions and guided surface waves for a surface conductivity model of graphene," *J. Appl. Phys.* **103**(6), 064302 (2008).
33. M. Jablan, H. Buljan, and M. Soljacic, "Plasmonics in Graphene at Infrared Frequencies," *Phys. Rev. B* **80**(24), 245435 (2009).
34. A. H. C. Neto, F. Guinea, N. M. R. Peres, K. S. Novoselov, and A. K. Geim, "The Electronic Properties of Graphene," *Rev. Mod. Phys.* **81**(1), 109–162 (2009).
35. S. Pechprasarn, S. Learkthanakhachon, G. G. Zheng, H. Shen, D. Y. Lei, and M. G. Somekh, "Grating-coupled Otto configuration for hybridized surface phonon polariton excitation for local refractive index sensitivity enhancement," *Opt. Express* **24**(17), 19517–19530 (2016).
36. D. R. Mason, S. G. Menabde, and N. Park, "Unusual Otto excitation dynamics and enhanced coupling of light to TE plasmons in graphene," *Opt. Express* **22**(1), 847–858 (2014).
37. M. F. Limonov, M. V. Rybin, A. N. Poddubny, and Y. S. Kivshar, "Fano resonances in photonics," *Nat. Photonics* **11**(9), 543–554 (2017).